ORIGINAL SCIENTIFIC PAPER

CROATICA CHEMICA ACTA

Croat. Chem. Acta **2018**, *91*(2), 187–193
Published online: June 7, 2018
DOI: 10.5562/cca3343

HKD 1926

The Mechanism of Peptide Hydrolysis Catalysed by Dipeptidyl Peptidase III from *Bacteroides thetaiotaomicron*

Marko Tomin,[1,*] Antonija Tomić,[1] Borislav Kovačević,[2] Sanja Tomić[1,#]

[1] Division of Organic Chemistry and Biochemistry, Ruđer Bošković Institute, Bijenička cesta 54, 10000 Zagreb, Croatia

[2] Division of Physical Chemistry, Ruđer Bošković Institute, Bijenička cesta 54, 10000 Zagreb, Croatia

* Corresponding author's e-mail address: marko.tomin@irb.hr

Corresponding author's e-mail address: sanja.tomic@irb.hr

RECEIVED: April 13, 2018 ✶ REVISED: May 10, 2018 ✶ ACCEPTED: May 15, 2018

THIS PAPER IS DEDICATED TO DR. BISERKA KOJIĆ-PRODIĆ ON THE OCCASION OF HER 80TH BIRTHDAY

Abstract: Dipeptidyl peptidase III (DPP III) is a zinc-dependent peptidase that cleaves dipeptides off of N-termini of its substrates. Previous studies on human DPP III reveal a reaction mechanism similar to that of thermolysin. Since the active site is conserved within the DPP III family, it is not surprising that the mechanism determined for *Bacteroides thetaiotaomicron* DPP III (*Bt*DPP III) closely resembles that of hDPP III. However, the hydrogen bond network within the model differs slightly from that in the human ortholog, which results in two proposed pathways. The calculated Gibbs activation energy of 90.1 kJ mol^{-1} is larger than the one calculated from kinetic data for the preferred substrate Arg_2-2-naphthylamide at room temperature (69 kJ mol^{-1}), suggesting the importance of treating the whole DPP III enzyme in the calculations.

Keywords: dipeptidyl peptidase III, DPP III, peptide hydrolysis, reaction mechanism, *Bacteroides thetaiotaomicron*.

INTRODUCTION

DIPEPTIDYL peptidases III (DPPs III) are zinc-dependent peptidases that cleave dipeptides off of N-termini of their substrates, namely peptides consisting of 3–8 amino acid residues.[1] According to the MEROPS database,[2] they belong to the M49 peptidase family which is characterized by five conserved regions.[3] Two of these five motifs, HEXXGH and E*EXR(K)AE(D) participate in the zinc ion coordination. The histidines from the first motive coordinate the metal ion as monodentate ligands and the Glu* from the second motive alternately as a flexible mono- or bidentate ligand.

As a predominantly cytosolic enzyme DPP III is thought to participate in the final steps of intracellular protein catabolism.[4] The mammalian enzyme participates in the defence against oxidative stress through activation of the Keap1-Nrf2 signalling pathway,[5,6] while recent studies on mice reveal a potential role in the blood pressure regulation.[7] The physiological role of DPP III in prokaryotes is not yet clear, however, the studies on *Caldithrix abyssi* (*Ca*) and *Porphyromonas gingivalis* (*Pg*) revealed the products of DPP III hydrolysis as an important source of nutrition for these microorganisms,[8–10] stressing the importance of peptidases in their metabolic pathways. Further on, *Pg*DPP IV has been reported to effect the connective tissue degradation, thus increasing the *Pg* pathogenicity.

Bacteroides thetaiotaomicron (*Bt*) is a Gram-negative anaerobe and a predominant member of the intestinal microbiota in mammals,[11,12] where it plays an important role in lactose[13] and certain glycans' degradation.[14] Although *B. thetaoitaomicron* increases both innate and acquired immunity,[15,16] it is also an opportunistic pathogen, resistant to the wide range of antibiotics.[17,18] In view of the new findings on the role of DPP III in the defence against oxidative stress in mammals, the potential effect on aerotolerance in anaerobic opportunistic pathogens such as *B. thetaiotaomicron* is of interest for clinical investigations.[19]

Crystal structures of *Bt*DPP III (PDB codes: 5NA7 and 5NA8) reveal a two-domain protein whose domains are

subject to the long-range conformational changes, from the so-called "open" to the "closed" form.[20,21] This is in line with previously reported results for the human ortholog,[22] where the closed enzyme form has been identified as the catalytically active.[23,24] The zinc-binding site is located in the upper domain, along with the DPP III trademark motives HECLGH and EEARAD. Long MD simulations of DPP III orthologs with various substrates revealed that the lowest-energy binding mode is the one with the substrate bound in the vicinity of the conserved ^{383}GINL β-sheet (Figure 1).[21,25,26]

A mechanism of the peptide bond hydrolysis in the human ortholog has recently been proposed.[27] It is based on the similarity of the DPP III active site with that of the enzyme thermolysin,[28] whose catalytic mechanism had been studied earlier.[29] According to Tomić *et al.*, the reaction rate is controlled by the first two steps, the glutamate-assisted water nucleophilic attack and the subsequent nitrogen inversion.[27] However, due to the lack of any crystal structure of *Bt*DPP III – substrate complexes and the significantly different substrate affinity between hDPP III and *Bt*DPP III (for example k_{cat} values for the preferred synthetic substrate Arg_2-2-naphthylamide are 21.8 and 5.0 s^{-1}, respectively),[30,31] we felt prompted to investigate the *Bt*DPP III reaction mechanism.

EXPERIMENTAL

The *Bt*DPP III active site model was prepared manually based on the open *Bt*DPP III crystal structure (PDB code: 5NA7),[20] the crystal structure of the hDPP III complex with leu-enkephalin (PDB code: 5E3A)[32] used in previous QM/MM studies[27] and the complex with Arg_2-2-naphthylamide (RRNA) obtained from long MD simulations.[21] The model consists of the zinc ion, necessary for the catalytic activity,[33] His448, His453 and Glu476 which coordinate the zinc ion,[3,34] a water molecule required for the peptide bond hydrolysis, Glu449 which activates the water molecule according to the mechanism proposed for the human ortholog,[27] His533 and Tyr309 taking part in the substrate stabilization[21,27] and a model substrate CH_3CO-Gly-$NHCH_3$ (Figure 2). His448 and His453 were kept neutral, with their Nδ sites protonated, whereas His533 was in protonated state since QM/MM studies on the human ortholog show that the reaction is not feasible with neutral His568 analogous to His533 in *Bt*DPP III.[27] All the residues were capped by replacing the Cβ atom with a methyl group whose coordinates were restrained. The system was described using the B97D functional[35] in conjunction with the 6-31G(d) basis set for C, H, N and O atoms, whereas the zinc ion was described using the LANL2DZ-ECP basis set[36] since the previous works on the human ortholog were performed at the same level of theory.[27] B97D was chosen since it accounts for dispersion and has been successfully used to describe zinc-dependent metalloenzymes previously.[37] Further on, as a non-hybrid functional, it offers a good compromise between accuracy and computing time. The solvent was treated implicitly, using the PCM model with SMD corrections[38] and a default dielectric constant of water (78.39). All calculations were performed using the Gaussian 09 program package.[39]

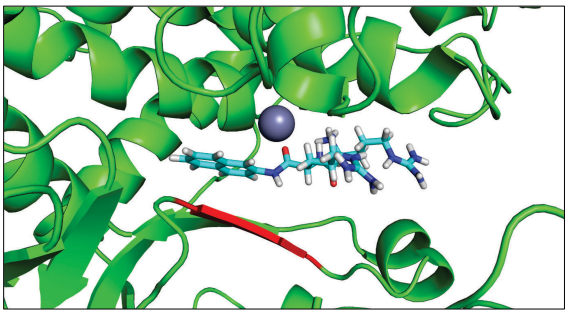

Figure 1. Arg_2-2-naphthylamide (RRNA) binding mode identified by long MD simulations.[21] The conserved ^{383}GINL β-sheet is shown in red, RRNA atoms as blue sticks and Zn^{2+} as a grey sphere. The figure was prepared using the PyMOL program.[43]

RESULTS AND DISCUSSION

In the optimized structure of the enzyme-substrate complex model (ES), the zinc ion is coordinated by His448, His453, Glu476 and one water molecule (Figure 2), bringing its coordination to 4, which is in line with previous results of QM/MM calculations on the human DPP III.[27] The carbonyl group from the scissile peptide bond of the model substrate, namely the O_s atom, is in the vicinity of the Zn^{2+} ion, but not within its coordination sphere (3.24 Å). The water molecule, required for the peptide bond hydrolysis, is strongly polarized by the carboxyl group of Glu449, which is reflected in the O_w–H_w and H_w–O_e distances (Table S1). Evolutionally conserved His533 and Tyr309 stabilize the substrate; His533 through the hydrogen bond between Nε

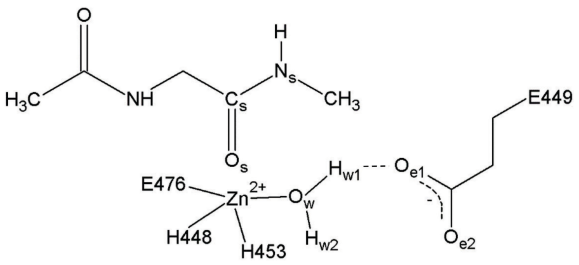

Figure 2. Minimal model of the *Bt*DPP III active site with the model substrate. His533 and Tyr309 have been omitted for clarity.

and O_s, while the hydroxyl group of Tyr309 interacts with the substrate backbone.

Nucleophilic Water Addition

Like in the case of human ortholog, the first reaction step involves Glu449-assisted nucleophilic addition of the hydroxyl group to the scissile peptide bond carbonyl group (Figure 3). The subsequent change in the C_s hybridization results in O_s entering the Zn^{2+} ion coordination sphere, while the O_w–Zn distance increases (Table S1). The role of the conserved His533 is twofold; its Nε atom forms a hydrogen bond with the carbonyl oxygen O_s which both decreases the density of the negative charge within the carbonyl group and positions it in a way that allows for a nucleophilic attack to occur (O_s–C_s–O_w angle is 83.7° in the identified enzyme-substrate complex). This reaction step has the highest Gibbs activation energy of 90.1 kJ mol^{-1}. The role of the zinc ion in stabilizing the oxyanion is reflected in the rapid drop of the O_s-Zn distance in the TS1 transition state. O_s entrance in the Zn^{2+} coordination sphere is accompanied by a significant distortion of the planar structure present in the ES complex, as noted by changes in the O_w-C_s distance and ω_1 and ω_2 values, ultimately resulting in a tetrahedral geometry present in INT1.

Nitrogen Inversion

The configuration of the N_s atom in the INT1 intermediate does not allow for a proton transfer from the Glu449 due to steric reasons (Figure 3). The inversion of the N_s atom

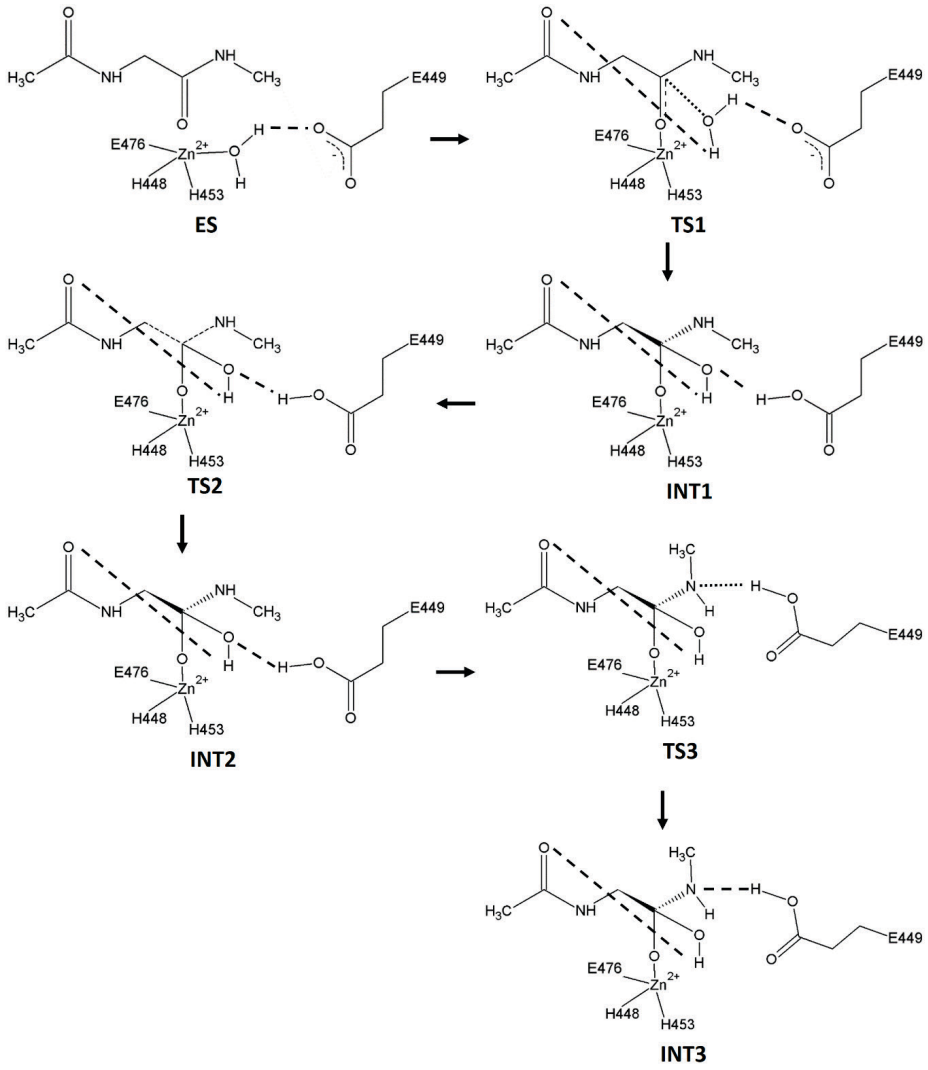

Figure 3. Reaction mechanism of the Glu449-assisted water addition and nitrogen inversion. Reaction intermediates are denoted as INT*n* and transition states as TS*n*. Hydrogen bonds are shown as dashed lines, while the bonds in the process of formation or cleavage are represented by dotted lines. His533 and Tyr309 have been omitted for clarity.

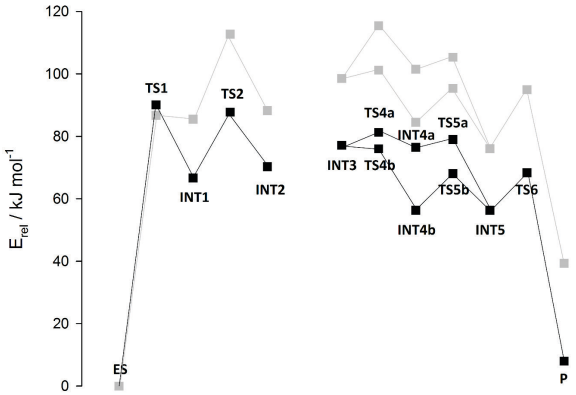

Figure 4. Energy profile for the amide bond hydrolysis in the *Bt*DPP III active site model calculated at the B97D/[6-31G(d) + LANL2DZ-ECP] level of theory. Electronic energies are shown as grey squares; estimated Gibbs energies at room temperature shown as black squares.

configuration (nitrogen inversion) is required in order to orient the N_s lone pair towards the protonated Glu449 (Figure 3). Such a transformation is usually a rapid process, with the inversion energy of trimethylamine (at 300 K) being about 34.7 kJ mol^{-1}.[40] The inversion occurs through a nearly planar transition state (ω_1 in TS2 is 171.9°), with the activation barrier of 21.1 kJ mol^{-1}. The structures INT1 and INT2 differ solely in the N_s atom configuration. According to the energy profile (Figure 4), the *R* isomer (INT1) is 3.7 kJ mol^{-1} more stable than the *S* isomer (INT2), while the energy barrier for INT2 to INT1 reversal is 17.4 kJ mol^{-1}. In case of the human DPP III a translocation of the Glu451 (Glu449 in *Bt*DPP III), accompanied by formation of two hydrogen bonds, was proposed as a way of inhibiting the reversal of INT2 to INT1.[27] Although we were not able to identify the transition state for this transformation within the model system used, the same behaviour was assumed. However, unlike the human ortholog, the hydrogen bond between H_{w2} and the carbonyl oxygen atom was preserved in INT3 (Figure 3, Table S1). As a result, two possible N_s protonation pathways were considered: one where the C_s-O_w bond rotation and formation of the H_{w2}-O_{e2} hydrogen bond precede the proton transfer from Glu449 to N_s and the other where protonation occurs before the H_{w2}–O_{e2} hydrogen bond formation (Figure 5). According to our calculations, the proton transfer from Glu449 to N_s followed by the C_s–O_w bond rotation result in a lower energy pathway than the alternative (Figures 4 and 5) due to the lower energies of the TS4b and TS5b transition states. When Gibbs energies at room temperature are compared, which include the zero-point energy and the thermal effects of vibration, the transition from INT3 to INT4b became barrierless. Also, except for TS1, energies of all transition states and intermediates significantly decrease.

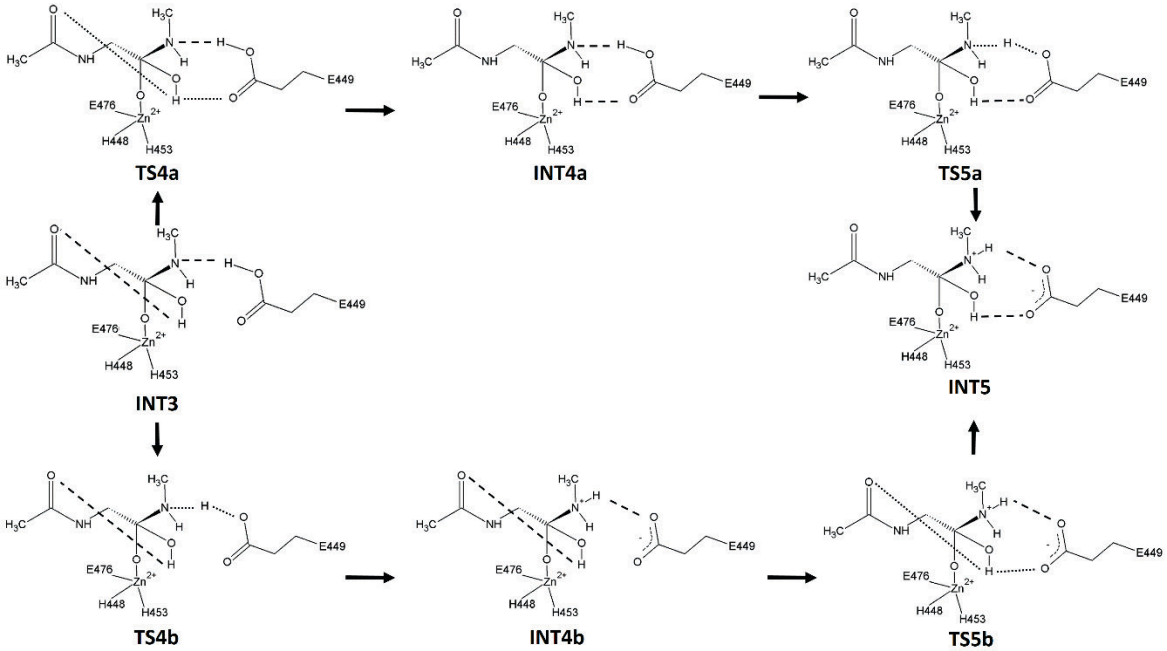

Figure 5. Two possible pathways from INT3 to INT5. Reaction intermediates are denoted as INT*n* and transition states as TS*n*. Hydrogen bonds are shown as dashed lines, while the bonds in the process of formation or cleavage are represented by dotted lines. His533 and Tyr309 have been omitted for clarity.

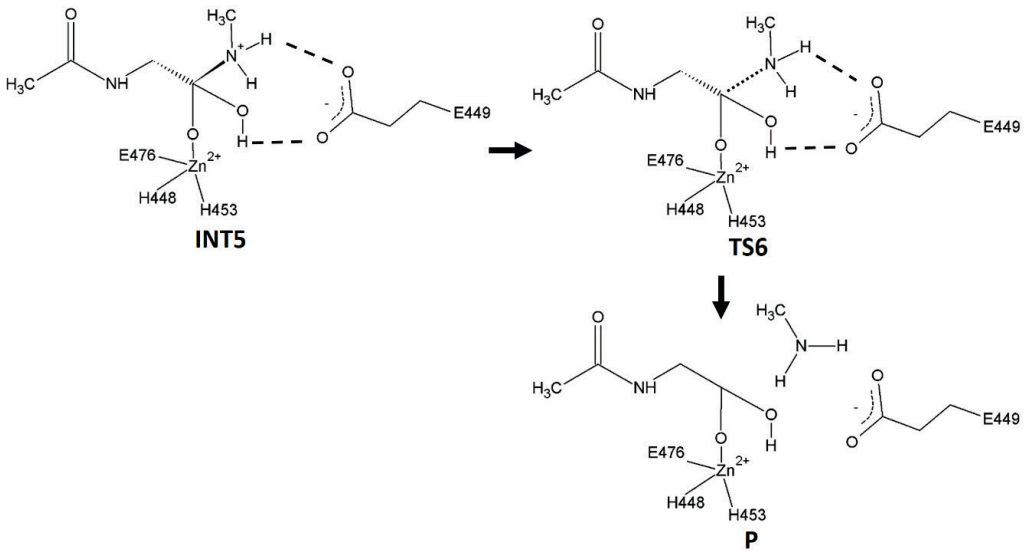

Figure 6. Reaction mechanism of the C_s-N_s bond cleavage. Hydrogen bonds are shown as dashed lines, while the bonds in the process of formation or cleavage.

It should be noted that N_s–C_s has a partial double bond character (d(C_s–N_s)=1.34 Å) in the ES complex while in the intermediates INT1-INT3 and INT4a it has the single bond character. The proton transfer from Glu449 to N_s significantly affects this bond, resulting in its elongation by 0.1 Å. All intermediates and transition states are stabilized by a hydrogen bond with the Nε-bound proton of His533, while Tyr309 stabilizes the substrate to a minor degree.

Amide Bond Cleavage

Unlike for the human ortholog where the proton transfer and the amide bond cleavage occur concertedly,[27] in the case of *Bt*DPP III the intermediate containing the protonated amino- group (INT5) was identified (Figure 6). The conformation of INT5 satisfies the stereoelectronic criteria according to Deslongchamps, *i.e.* the O_s and O_w atoms (bound to C_s) both have lone-pair orbitals antiperiplanar to the scissile C_s–N_s bond.[41] The subsequently formed methylamine is stabilized through the hydrogen bond with the carboxyl group of Glu449. The next steps in product formation would be the proton transfer from O_w to the newly formed amine, as suggested in case of thermolysin.[42] In the case of hDPP III this resulted with O_w entering the Zn^{2+} coordination sphere (wherein O_s moves out of the zinc coordination sphere) and establishing the initial coordination of the metal ion.[27] However, these reaction steps are not crucial for understanding the peptide bond cleavage and as such are not discussed in this paper.

Differently from the reaction determined for the human DPP III, where the rate is determined by the first and the second reaction step, in the case of *Bt*DPP III the peptide hydrolysis is determined by the first step solely, the Glu449-assisted water addition. The respective Gibbs activation energy (90.1 kJ mol^{-1}) is higher than the activation energy derived from the experimental data reported by Vukelić et al. for the preferred synthetic substrate Arg_2-2-naphthylamide, k_{cat} of 5.0 s^{-1}.[30] Despite

Table 1. Relative Gibbs energies for the intermediates and transition states proposed for the *Bt*DPP III catalysed peptide bond hydrolysis at room temperature.

	ΔG_{rel} / kcal mol^{-1}
ES	0.0
TS1	90.10
INT1	66.68
TS2	87.78
INT2	70.35
INT3	77.18
TS4a	81.31
TS4b	76.02
INT4a	76.45
INT4b	56.36
TS5a	78.99
TS5b	68.08
INT5	56.33
TS6	68.39
P	8.012

the different substrates, in the model system and the experiment, the obtained energy prompts additional computational studies of the *Bt*DPP III substrate binding.

CONCLUSION

The mechanism of the peptide bond hydrolysis catalysed by the DPP III from *Bacteroides thetaiotaomicron* was investigated using QM calculations on a model system constructed from the available *Bt*DPP III crystal structure and molecular docking results. The main steps in the peptide bond hydrolysis are the Glu449-assisted water addition, the inversion of the configuration on the amide nitrogen atom, its protonation and C−N bond cleavage.

According to our calculations the rate-determining step of the peptide hydrolysis reaction catalysed by *Bt*DPP III is the Glu449-assisted water addition. The translocation of Glu449 and subsequent locking of the nitrogen atom configuration immediately after its inversion, proposed in case of the human ortholog, was not observed in the *Bt*DPP III catalysed reaction. The preferred pathway seems to be the one where the amide nitrogen protonation occurs first, with the second substrate-Glu449 hydrogen bond forming in a separate step. Further on, the protonation of the amide nitrogen and the C-N bond cleavage are not concerted like in case of human DPP III.

The difference between the calculated Gibbs activation energy of the rate-determining step and the available experimental data underline the difficulty of creating a simple model of such a plastic active site. Our results stress the need for inclusion of the entire protein in further calculations and are in line with the significant difference in results obtained by QM and QM/MM approaches in previous studies on the human ortholog.

REFERENCES

[1] M. Chen, A. J. Barrett, *Handbook of Proteolytic Enzymes*, 2. ed., Elsevier, London, **2004**, 809–812.

[2] N. D. Rawlings, A. J. Barrett, R. Finn, *Nucleic acids research* **2015**, *44*, D343.

[3] M. Abramić, J. Špoljarić, Š. Šimaga, *Period Biol.* **2004**, *106*, 161.

[4] M. Abramić, M. Zubanović, L. Vitale, *Biol. Chem. Hoppe-Seyler* **1988**, *369*, 29.

[5] Y. Liu, J. T. Kern, J. R. Walker, J. A. Johnson, P. G. Schultz, H. Luesch, *Proc Natl Acad Sci U S A* **2007**, *104*, 5205.

[6] B. E. Hast, D. Goldfarb, K. M. Mulvaney, M. A. Hast, P. F. Siesser, F. Yan, D. N. Hayes, M. B. Major, *Cancer Res.* **2013**, *73*, 2199.

[7] X. Pang, A. Shimizu, S. Kurita, D.P. Zankov, K. Takeuchi, M. Yasuda-Yamahara, S. Kume, T. Ishida, H. Ogita, *Hypertension* **2016**, *68*, 630.

[8] I. V. Kublanov, O. M. Sigalova, S. N. Gavrilov, A. V. Lebedinsky, C. Rinke, O. Kovaleva, N. A. Chernyh, N. Ivanova, C. Daum, T. B. Reddy *et al.*, *Front Microbiol.* **2017**, *8*, 195.

[9] T. K. Nemoto, Y. Ohara-Nemoto, *Japanese Dental Science Review* **2016**, *52*, 22.

[10] T. K. Nemoto, Y. Ohara-Nemoto, G. A. Bezerra, Y. Shimoyama, S. Kimura, *J. Biol. Chem.* **2016**, *291*, 5913.

[11] L. E. Comstock, M. J. Coyne, *Bioessays* **2003**, *25*, 926.

[12] J. Xu, M. K. Bjursell, J. Himrod, S. Deng, L. K. Carmichael, H. C. Chiang, L. V. Hooper, J. I. Gordon, *Science* **2003**, *299*, 2074.

[13] G. A. O'Toole, *J Bacteriol.* **2016**, *198*, 2763.

[14] D. Ndeh, A. Rogowski, A. Cartmell, A. S. Luis, A. Basle, J. Gray, I. Venditto, J. Briggs, X. Zhang, A. Labourel *et al.*, *Nature* **2017**, *544*, 65.

[15] M. A. Zocco, M. E. Ainora, G. Gasbarrini, A. Gasbarrini, *Digestive and Liver Disease* **2007**, *39*, 707.

[16] L. V. Hooper, J. Xu, P. G. Falk, T. Midtvedt, J. I. Gordon, *Proc. Natl. Acad. Sci.* **1999**, *96*, 9833.

[17] I. Brook, *Expert Rev. Anti Infect Ther.* **2007**, *5*, 991.

[18] E. Nagy, E. Urbán, *Clinical Microbiology and Infection* **2011**, *17*, 371.

[19] P. Y. Tang, M. M. Dallas, M. H. Malamy, *Mol Microbiol.* **1999**, *32*, 139.

[20] I. Sabljić, N. Meštrović, B. Vukelić, P. Macheroux, K. Gruber, M. Luić, M. Abramić, *PLOS ONE* **2017**, *12*, e0187295.

[21] M. Tomin, S. Tomić, *Molecular BioSystems* **2017**, *13*, 2407.

[22] G. A. Bezerra, E. Dobrovetsky, R. Viertlmayr, A. Dong, A. Binter, M. Abramić, P. Macheroux, S. Dhe-Paganon, K. Gruber, *Proc Natl Acad Sci U S A* **2012**, *109*, 6525.

[23] A. Tomić, M. Gonzalez, S. Tomić, *J Chem Inf Model* **2012**, *52*, 1583.

[24] A. Tomić, S. Tomić, *Dalton Trans* **2014**, *43*, 15503.

[25] I. Sabljić, M. Tomin, M. Matovina, I. Sučec, A. Tomašić Paić, A. Tomić, M. Abramić, S. Tomić, *PloS One* **2018**, *13*, e0192488.

[26] A. Tomić, M. Berynskyy, R. C. Wade, S. Tomić, *Mol. Biosyst.* **2015**, *11*, 3068.

[27] A. Tomić, B. Kovačević, S. Tomić, *Phys. Chem. Chem. Phys.* **2016**, *18*, 27245.

[28] P. K. Baral, N. Jajčanin-Jozić, S. Deller, P. Macheroux, M. Abramić, K. Gruber, *J. Biol. Chem.* **2008**, *283*, 22316.

[29] J. Blumberger, G. Lamoureux, M. Klein, *J. Chem. Theory Comput.* **2007**, *3*, 1837.

[30] B. Vukelić, B. Salopek-Sondi, J. Špoljarić, I. Sabljić, N. Meštrović, D. Agić, M. Abramić, *Biol. Chem.* **2012**, *393*, 37.

[31] J. Špoljarić, B. Salopek-Sondi, J. Makarević, B. Vukelić, D. Agić, Š. Šimaga, N. Jajčanin-Jozić, M. Abramić, *Bioorg. Chem.* **2009**, *37*, 70.
[32] P. Kumar, V. Reithofer, M. Reisinger, S. Wallner, T. Pavkov-Keller, P. Macheroux, K. Gruber, *Sci. Rep.* **2016**, *6*, 23787.
[33] K. Fukasawa, K. M. Fukasawa, M. Kanai, S. Fujii, J. Hirose, M. Harada, *Biochem. J.* **1998**, *329*, 275.
[34] K. Fukasawa, K. M. Fukasawa, H. Iwamoto, J. Hirose, M. Harada, *Biochemistry* **1999**, *38*, 8299.
[35] S. Grimme, *J. Comput. Chem.* **2006**, *27*, 1787.
[36] P. J. Hay, W. R. Wadt, *J. Chem. Phys.* **1985**, *82*, 299.
[37] N. Gresh, K. El Hage, D. Perahia, J. P. Piquemal, C. Berthomieu, D. Berthomieu, *J. Comput. Chem.* **2014**, *35*, 2096.
[38] A. V. Marenich, C. J. Cramer, D. G. Truhlar, *J. Phys. Chem. B* **2009**, *113*, 6378.
[39] Gaussian 09 (Versions A. 01 and D. 01), M. Frisch, G. Trucks, H. Schlegel, G. Scuseria, M. Robb, J. Cheeseman, G. Scalmani, V. Barone, B. Mennucci, G. Petersson, Gaussian, Inc., Wallingford CT, **2009**.
[40] A. M. Halpern, M. J. Ondrechen, L. D. Ziegler, *J. Am. Chem. Soc.* **1986**, *108*, 3907.
[41] P. Deslongchamps, *Tetrahedron* **1975**, *31*, 2463.
[42] V. Pelmenschikov, M. Blomberg, P. Siegbahn, *J. Biol. Inorg. Chem.* **2002**, *7*, 284.
[43] The PyMOL Molecular Graphics System, Version 1.8 Schrödinger, LLC, 2017.